International Journal of Solids and Structures 56–57 (2015) 11–19

Contents lists available at ScienceDirect

International Journal of Solids and Structures

journal homepage: www.elsevier.com/locate/ijsolstr

Isotropic to distortional hardening transition in metal plasticity

Niko Manopulo [a,*], Frédéric Barlat [b], Pavel Hora [a]

[a] Institute of Virtual Manufacturing, Swiss Federal Institute of Technology (ETH Zurich), Tannenstrasse 3, 8092 Zurich, Switzerland
[b] On leave from Graduate Institute of Ferrous Technology (GIFT), Pohang University of Science and Technology (POSTECH), San 31, Hyoja-dong, Nam-gu, Pohang, Gyeongbuk 790-784, Republic of Korea

ARTICLE INFO

Article history:
Received 30 July 2014
Received in revised form 13 October 2014
Available online 24 December 2014

Keywords:
Distortional hardening
Bauschinger effect
Latent hardening
HAH

ABSTRACT

The present paper aims to discuss the transition from isotropic to distortional hardening behavior of metallic materials, based on the Homogeneous Anisotropic Hardening (HAH) model. Furthermore, the effect of yield locus distortion on the evolution of the strain increment, under the assumption of associated flow, is theoretically discussed and exemplified. Special cases, such as coaxial and orthogonal stress states, are analyzed to provide better insight into the model. Particular emphasis is put on the monotonic loading case, which is compared to isotropic hardening. Finally, the evolution equations of the state variables are examined and their properties are discussed.

1. Introduction

The materials used in automotive industry are rapidly evolving. Policy decisions for manufacturing energy efficient products on the one hand, and continuously increasing requirements on passenger safety on the other, drive the industry towards using materials with a high strength-to-weight ratio. This, in turn, spurns the development of Advanced High Strength Steels (AHSS) as well as lighter metals such as aluminum and magnesium alloys. The latter not only exhibit strong initial anisotropy, they are also subject to significant loading path dependence. Microstructure driven mechanisms such as the Bauschinger effect and latent hardening/softening, thus become important and need to be considered in modeling these materials.

Distortional hardening models have received attention since many years, early approaches such as the ones proposed Ortiz and Popov (1983) and Voyiadjis and Foroozesh (1990) described a change in the shape of the yield locus with plastic deformation. A more complex model has been proposed by Kurtyka and Zyczkowski who considered affine deformation and rotation in addition to proportional expansion, translation and distortion (Kurtyka and Zyczkowski, 1996). Another comprehensive model, including isotropic, kinematic and directional hardening effects has been proposed in a series of works by Feigenbaum and Dafalias (2007, 2008) and Dafalias and Feigenbaum (2011) as well as Aretz (2008). More recently Shutov and Ihlemann suggested a viscoplasticity approach for the description of distortional hardening phenomena (Shutov and Ihlemann, 2012). Experimental analysis of distortional hardening has been published by Phillips et al. (1972) and more recently in two contributions by Khan et al., for an aluminium alloy deformed under proportional and non proportional loading conditions (Khan et al., 2009, 2010). Subsequently, Pietryga et al. used a finite deformation model to investigate these effects and discussed their agreement with experiments (Pietryga et al., 2012).

There have been numerous efforts in modeling the Bauschinger effect. A comprehensive review can be found in Chaboche (2008). Modelling approaches for the specific case of sheet forming can be found in Yoshida et al. (2002), Yoshida and Uemori (2002) and Yoshida and Uemori (2003). A tensorial description of dislocation structures which evolve with plastic deformation has been proposed by Teodosiu and Hu (1998). This effect has been also thoroughly investigated at the crystal plasticity level (see e.g. by Peeters et al. (2000, 2001), Franz et al. (2009) and Kitayama et al. (2013)).

The Homogeneous Anisotropic Hardening (HAH) model has been first proposed in 2011 (Barlat et al., 2011) for capturing the Bauschinger effect and subsequently extended and revised to include latent effects (Barlat et al., 2013, 2014). In contrast to earlier methods, which are mostly based on the concept of kinematic hardening, the HAH model provides a modular framework for the description of anisotropy, Bauschinger and latent effects, either independently or combined in an arbitrary manner. This releases restrictions about the use of particular yield loci or hardening models on the one hand and enables the extension of

* Corresponding author.
E-mail address: manopulo@ivp.mavt.ethz.ch (N. Manopulo).

http://dx.doi.org/10.1016/j.ijsolstr.2014.12.015
0020-7683/

existing models in order to account for microstructural effects on the other.

The HAH model has been used in the recent literature in order to investigate the role of microstructure effects on different processes. Lee et al. (2012) used the model to investigate the role of the Bauschinger effect on springback for U-draw/bending of pre-strained material. Lee et al. (2012) compared the accuracy of springback prediction of the HAH model with that of the Chaboche kinematic hardening model. He et al. (2013) proposed an extension to the original HAH model able to capture work hardening stagnation and cross-effects, by introducing four new parameters. A meso-scale simulation approach has been proposed by Ha et al. (2014) which uses the model in combination to a crystal plasticity approach in order to investigate the behavior of dual-phase steels. The effect of continuous versus abrupt strain path change has been investigated in another contribution by Ha et al. (2014), who also tested the ability of the model to capture the rate of path change from plane strain to simple shear. The effect of cyclic loading on fatigue prediction of low carbon sheet steel has been studied by Hariharan et al. (2014). Lee et al. introduced a dislocation density based hardening model into the HAH framework and tested the results related to springback accuracy. Similarly Lee et al. (2013) proposed an extension of the quasi-plastic elastic approach by incorporating nonlinear elasticity effects to improve the accuracy in springback prediction.

The present contribution primarily aims to discuss, based on the HAH model, the transition between isotropic and distortional hardening responses in case of non-proportional loading. In addition, it is rigorously proven, that the response of the HAH model for the case of proportional loading is strictly identical to that of the classical anisotropic yield function under isotropic hardening. This is valid for the general case, including asymmetric yield loci, with the only restriction being the homogeneity of the stable component, as this is a defining property of the HAH model itself. The proof is achieved through a semi-geometric re-interpretation of the model, which in turn provides insight into the different model features and is expected to facilitate the understanding and application of the methodology.

2. Interpretation of original HAH model

In this section, the different state variables and coefficients controlling the Bauschinger effect in the HAH approach will be revised and investigated, in order to provide better insight into the model. The evolution laws for these variables are reviewed in Section 5.

2.1. Yield condition

The HAH yield condition can be written as follows:

$$\bar{\sigma}^q(\mathbf{s}) = \phi^q(\mathbf{s}) + f_-^q \phi_-^q(\mathbf{s}) + f_+^q \phi_+^q(\mathbf{s}) = \sigma_r^q \tag{1}$$

where ϕ is any positively homogeneous yield function, $\mathbf{s}$ is the stress deviator, q is a blending exponent and σ_r is a reference stress (e.g. uniaxial tensile stress). The state variables f_+ and f_-[1] enable the distortion of the yield locus and must stay positive in order to guarantee convexity of the yield surface. The functions ϕ_+ and ϕ_- quantify the strength of load reversal and are defined as follows:

$$\begin{aligned} \phi_- &= \left| \hat{\mathbf{h}} : \mathbf{s} - \left| \hat{\mathbf{h}} : \mathbf{s} \right| \right| \\ \phi_+ &= \left| \hat{\mathbf{h}} : \mathbf{s} + \left| \hat{\mathbf{h}} : \mathbf{s} \right| \right| \end{aligned} \tag{2}$$

[1] Note that the notation in Eq. (1) slightly differs from previous publications. The correspondence is such that $f_- = f_1$ and $f_+ = f_2$ and similarly for the other state variables.

where the second order tensor $\hat{\mathbf{h}}$ is called the microstructure deviator and captures the loading history of the material. Its initial value corresponds to the normalized stress deviator at the first plastic strain increment and subsequently evolves according to the laws given in Section (5). Furthermore, this quantity is defined in a manner that its size (as measured by the norm $x = \|\mathbf{x}\| = \sqrt{\mathbf{x} : \mathbf{x}}$) always corresponds to $1/\sqrt{H}$. The normalization parameter H simply represents an arbitrary size and does not influence the model. A normalized version of the stress deviator is also similarly defined:

$$\hat{\mathbf{s}} = \frac{\mathbf{s}}{\sqrt{H\mathbf{s} : \mathbf{s}}} = \frac{1}{\sqrt{H}} \frac{\mathbf{s}}{\|\mathbf{s}\|} = \frac{1}{s\sqrt{H}} \mathbf{s} \tag{3}$$

2.2. Interpretation of $\hat{\mathbf{h}} : \mathbf{s}$

The central quantity in the formulation is the double dot product between the microstructure deviator $\hat{\mathbf{h}}$ and the deviatoric stress tensor $\mathbf{s}$. Geometrically speaking, this can be interpreted as the projection of the stress deviator on the axis defined by the microstructure deviator. This, in turn, provides twofold information about the current stress state with respect to the loading history:

Sign of $\hat{\mathbf{h}} : \mathbf{s}$.

- If $\hat{\mathbf{h}} : \mathbf{s} > 0$ the loading path may have changed direction, but loading has not been reversed. New slip systems are activated but none of the already active slip systems are likely working in the reverse direction.
- If $\hat{\mathbf{h}} : \mathbf{s} < 0$ New slip systems are activated but also some of the active slip systems are active in the reverse direction.
- If $\hat{\mathbf{h}} : \mathbf{s} = 0$ cross loading. None of the previously active slip systems are active in the second deformation step.

Size of $\hat{\mathbf{h}} : \mathbf{s}$.

The quantity $\hat{\mathbf{h}} : \mathbf{s}$ is also related to the "angle" χ between the two tensors. In fact, by using the definition of the angle between two tensors, the latter is defined as:

$$\cos\chi = \frac{\hat{\mathbf{h}} : \mathbf{s}}{\|\hat{\mathbf{h}}\| \|\mathbf{s}\|} = \frac{\sqrt{H}}{s} \hat{\mathbf{h}} : \mathbf{s} = H \hat{\mathbf{h}} : \hat{\mathbf{s}} \tag{4}$$

It is worthwhile to note that the stress deviator can change direction arbitrarily and even abruptly, whereas the microstructure deviator only evolves progressively, as a function of the plastic work, and realigns itself along the stress deviator axis. This property of the model ensures that the yield locus shape remains primarily a function of the prior deformation history and not of the instantaneous stress state. To clarify this point let us assume that $\hat{\mathbf{h}}$ and $\mathbf{s}$ are diagonal and that $\hat{\mathbf{h}} : \mathbf{s} = 0$ at the instant of the load change (i.e. cross-loading). If there is latent hardening, this change translates physically by an overshooting of the flow stress with respect to the monotonic hardening curve. If the new load is such that, instead of being diagonal, $\mathbf{s}$ contains shear components, $\hat{\mathbf{h}} : \mathbf{s}$ is still equal to 0. This means that, at the very moment of the change, the yield surface is the same for these two cases. However, the actual material response will depend on the actual stress applied in the second segment, i.e., with or without shear components. In addition, the absolute value of the off-diagonal components of h starts to increase but only gradually because the microstructure does not change suddenly.

2.3. Interpretation of ϕ_+ and ϕ_-

The HAH model in (1) is devised in a manner that depending on the sign of $\hat{\mathbf{h}} : \mathbf{s}$, only one of the functions ϕ_+ and ϕ_- is active. In fact it is easily seen in Eq. (2), that the following holds:

$$\phi_+ = \begin{cases} 2\hat{\mathbf{h}} : \mathbf{s} & \text{if } \hat{\mathbf{h}} : \mathbf{s} \geqslant 0 \\ 0 & \text{if } \hat{\mathbf{h}} : \mathbf{s} \leqslant 0 \end{cases} \quad \phi_- = \begin{cases} 0 & \text{if } \hat{\mathbf{h}} : \mathbf{s} \geqslant 0 \\ -2\hat{\mathbf{h}} : \mathbf{s} & \text{if } \hat{\mathbf{h}} : \mathbf{s} \leqslant 0 \end{cases} \tag{5}$$

In case of monotonic loading, ϕ_+ is active but, as it is clarified in Section 2.4, the corresponding state variable f_+ is null, thus reducing the equivalent stress to be equal to the stable yield function ($\bar{\sigma} = \phi(\mathbf{s})$). In case of load reversal, ϕ_+ is null while ϕ_- is active and the yield stress depends on the value of f_-, which has been evolving during first deformation step. Using these observations, a more compact notation can be introduced, which will be used in the rest of this work. In fact, by defining $\epsilon \equiv \text{sgn}(\hat{\mathbf{h}} : \mathbf{s})$, Eq. (1) can be rewritten as follows:

$$\bar{\sigma}^q(\mathbf{s}) = \phi^q(\mathbf{s}) + \left(2f_\epsilon|\hat{\mathbf{h}} : \mathbf{s}|\right)^q = \sigma_r^q \tag{6}$$

Furthermore, using the second equality in Eq. (4) results in:

$$\bar{\sigma}^q(\mathbf{s}) = \phi^q(\mathbf{s}) + \left(2f_\epsilon \frac{s}{\sqrt{H}}|\cos\chi|\right)^q = \sigma_r^q \tag{7}$$

2.4. Interpretation of f_+ and f_-

In order to derive an expression for the state variables, the stress states on the stable yield surface $\mathbf{s}_{\epsilon i}$ (isotropic hardening) can be compared to the ones on the distorted surface $\mathbf{s}_{\omega d}$ (see Fig. 1). The notation ω (+/−) here is equivalent to ϵ and is introduced to stress that ω and ϵ are not necessarily equal. The expression for the stable yield locus thus becomes:

$$\bar{\sigma}(\mathbf{s}_{\epsilon i}) = \phi(\mathbf{s}_{\epsilon i}) = \phi(\sqrt{H}s_{\epsilon i}\hat{\mathbf{s}}_{\epsilon i}) = \sqrt{H}s_{\epsilon i}\phi(\hat{\mathbf{s}}_{\epsilon i}) = \sigma_r \tag{8}$$

where Eq. (3) as well as the homogeneity of ϕ have been used: similarly for the stress point on the distorted surface:

$$\bar{\sigma}(\mathbf{s}_{\omega d}) = \left[\phi^q(\mathbf{s}_{\omega d}) + \left(2f_\omega \frac{s_{\omega d}}{\sqrt{H}}|\cos\chi|\right)^q\right]^{\frac{1}{q}} = \sigma_r \tag{9}$$

Again, using (3) and the homogeneity of the functions:

$$\bar{\sigma}(\mathbf{s}_{\omega d}) = \left\{\left[\sqrt{H}s_{\omega d}\phi(\hat{\mathbf{s}}_{\omega d})\right]^q + \left(2f_\omega \frac{s_{\omega d}}{\sqrt{H}}|\cos\chi|\right)^q\right\}^{\frac{1}{q}} = \sigma_r \tag{10}$$

As both stress points refer to the same reference stress σ_r, equating Eqs. (10) and (8) leads to:

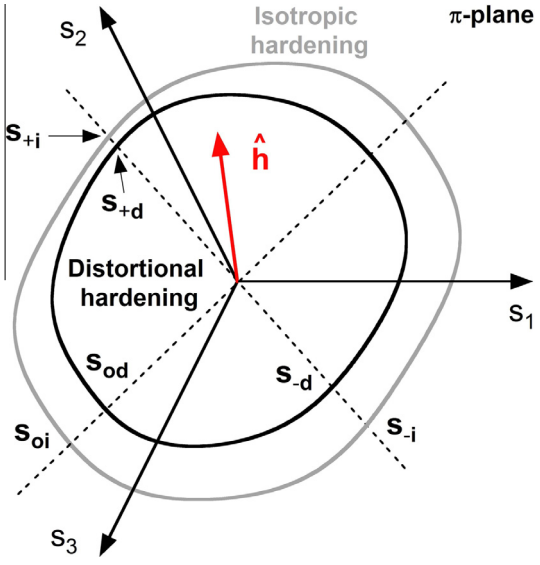

Fig. 1. Stress states on the stable and distorted yield loci.

$$\left[\sqrt{H}s_{\epsilon i}\phi(\hat{\mathbf{s}}_{\epsilon i})\right]^q = \left[\sqrt{H}s_{\omega d}\phi(\hat{\mathbf{s}}_{\omega d})\right]^q + \left(2f_\omega \frac{s_{\omega d}}{\sqrt{H}}|\cos\chi|\right)^q \tag{11}$$

Dividing both sides by $\left[\sqrt{H}s_{\omega d}\phi(\hat{\mathbf{s}}_{\omega d})\right]^q$ and reordering the terms, the following relation for f_ω is obtained:

$$f_\omega = \frac{H\phi(\hat{\mathbf{s}}_{\omega d})}{2|cos\chi|}\left[\left(\frac{s_{\epsilon i}}{s_{\omega d}}\frac{\phi(\hat{\mathbf{s}}_{\epsilon i})}{\phi(\hat{\mathbf{s}}_{\omega d})}\right)^q - 1\right]^{\frac{1}{q}} \tag{12}$$

This relationship is quite general, more useful expressions are derived in the following for specific cases.

2.4.1. Coaxial stress states

If the considered stress deviators are coaxial with the microstructure deviator i.e.,

$$\hat{\mathbf{s}}_{\epsilon i} = \epsilon\hat{\mathbf{h}}, \quad \hat{\mathbf{s}}_{\omega d} = \omega\hat{\mathbf{h}}, \quad |\cos\chi| = 1 \tag{13}$$

substituting into Eq. (12) leads to

$$f_\omega = \frac{H\phi(\omega\hat{\mathbf{h}})}{2}\left[\left(\frac{s_{\epsilon i}}{s_{\omega d}}\frac{\phi(\epsilon\hat{\mathbf{h}})}{\phi(\omega\hat{\mathbf{h}})}\right)^q - 1\right]^{\frac{1}{q}} \tag{14}$$

Note that Eq. (14) is valid for arbitrary non-symmetric yield loci, where the quantity $\phi(\epsilon\hat{\mathbf{h}})/\phi(\omega\hat{\mathbf{h}})$ is a measure for yield locus asymmetry. If centro-symmetry is assumed Eq. (14) reduces to:

$$f_\epsilon = \frac{H\phi(\epsilon\hat{\mathbf{h}})}{2}\left[\left(\frac{s_{\epsilon i}}{s_{\epsilon d}}\right)^q - 1\right]^{\frac{1}{q}} \tag{15}$$

By defining the stress ratio between distorted and isotropic hardening yield surfaces as a state variable $g_\epsilon = s_{\epsilon d}/s_{\epsilon i}$, Eq. (15) becomes:

$$f_\epsilon = \frac{H\phi(\epsilon\hat{\mathbf{h}})}{2}\left[\frac{1}{g_\epsilon^q} - 1\right]^{\frac{1}{q}} \tag{16}$$

2.4.2. Special cases

In this section the function f_ϵ is investigated for the common cases of uniaxial and balanced biaxial stress states.

Uniaxial tension.

For uniaxial tension with stress σ_t, the matrix representation of stress state reads:

$$[\boldsymbol{\sigma}_t] = \begin{bmatrix} \sigma_t & 0 & 0 \\ 0 & 0 & 0 \\ 0 & 0 & 0 \end{bmatrix} \quad [\mathbf{s}_t] = \begin{bmatrix} \frac{2}{3} & 0 & 0 \\ 0 & -\frac{1}{3} & 0 \\ 0 & 0 & -\frac{1}{3} \end{bmatrix}\sigma_t \tag{17}$$

Using Eqs. (8) and (13), the yield condition for isotropic hardening can be expressed as:

$$\bar{\sigma}(\mathbf{s}_t) = \sqrt{H}\|\mathbf{s}_t\|\phi(\epsilon\hat{\mathbf{h}}) = \sqrt{\frac{2H}{3}}\sigma_t\phi(\epsilon\hat{\mathbf{h}}) = \sigma_r \tag{18}$$

Rearranging the last equality:

$$\phi(\epsilon\hat{\mathbf{h}}) = \sqrt{\frac{3}{2H}}\frac{\sigma_r}{\sigma_t} \tag{19}$$

and substituting into (16), leads to

$$f_\epsilon = \sqrt{\frac{3H}{8}}\frac{\sigma_r}{\sigma_t}\left[\frac{1}{g_\epsilon^q} - 1\right]^{\frac{1}{q}} \tag{20}$$

Finally, assuming that the reference stress corresponds to the same tensile stress ($\sigma_r = \sigma_t$), Eq. (20) simplifies to:

$$f_\epsilon = \sqrt{\frac{3H}{8}}\left[\frac{1}{g_\epsilon^q} - 1\right]^{\frac{1}{q}} \tag{21}$$

This expression corresponds to Eq. (7) in the paper on HAH by Barlat et al. (2014), although the equation is written incorrectly in the

cited paper. Furthermore this equation justifies the choice made in Barlat et al. (2011) to set the parameter $H = 8/3$, as the vanishing square root simplifies the expression. Substituting (20) into (7) demonstrates that the parameter H does not influence the yield condition, which now becomes:

$$\bar{\sigma}^q(\mathbf{s}) = \phi^q(\mathbf{s}) + \left[\frac{1}{g_\epsilon^q} - 1\right]\left(\sqrt{\frac{3}{2}}s|\cos\chi|\right)^q = \sigma_r^q \tag{22}$$

2.4.3. Balanced biaxial tension

For balanced biaxial tension, with stress σ_b the following matrix representation applies:

$$[\boldsymbol{\sigma}_b] = \begin{bmatrix} \sigma_b & 0 & 0 \\ 0 & \sigma_b & 0 \\ 0 & 0 & 0 \end{bmatrix} \quad [\mathbf{s}_b] = \begin{bmatrix} \frac{1}{3} & 0 & 0 \\ 0 & \frac{1}{3} & 0 \\ 0 & 0 & -\frac{2}{3} \end{bmatrix}\sigma_b \tag{23}$$

This is formally identical to Eq. (17) and leads to the following expression:

$$f_\epsilon = \sqrt{\frac{3H}{8}}\frac{\sigma_r}{\sigma_b}\left[\frac{1}{g_\epsilon^q} - 1\right]^{\frac{1}{q}} \tag{24}$$

If, in addition, the reference stress is equal to the biaxial stress ($\sigma_r = \sigma_b$) Eq. (21) is recovered.

3. Interpretation of extended HAH model

So far, the properties of the HAH model based on load reversal only have been analyzed, without taking into consideration cross loading and latent effects. Furthermore the discussion about the state variables g_3 and g_4, used to capture permanent softening, has been omitted as their interpretation is trivial. This section deals with the properties of the extended model as proposed in Barlat et al. (2013, 2014), where two new state variables g_L and g_S are included in order to model latent hardening and shrinking effects respectively. The model postulates that, in case of cross loading (e.g. in case of two-step tension where the stress deviators of the two steps are orthogonal), none of the active slip systems stay active, such that no Bauschinger effect occurs. Similarly cross-loading is the case in which latent effects are maximized. A stress state can be decomposed into its components being coaxial and orthogonal to the previous loading state, represented by the microstructure deviator $\hat{\mathbf{h}}$. Note that this feature of the model allows for a clear uncoupling of the Bauschinger parameters from the latent hardening coefficients. In fact, the coefficients for the former can be identified independently from those of the latter, to capture either effect exclusively.

3.1. Decomposition of the stress deviator

Analogously to vector algebra, the component of $\mathbf{s}$ coaxial to $\hat{\mathbf{h}}$ is derived as follows:

$$\mathbf{s_c} = \|\mathbf{s}\|\cos\chi\frac{\hat{\mathbf{h}}}{\|\hat{\mathbf{h}}\|} = \frac{\mathbf{s}:\hat{\mathbf{h}}}{\|\hat{\mathbf{h}}\|^2}\hat{\mathbf{h}} = H(\hat{\mathbf{h}}:\mathbf{s})\hat{\mathbf{h}} \tag{25}$$

The orthogonal component can thus be easily calculated by subtracting the coaxial component from the stress deviator.

$$\mathbf{s_o} = \mathbf{s} - \mathbf{s_c} \tag{26}$$

3.2. Extended yield condition

The extended yield condition proposed in Barlat et al. (2014) is:

$$\bar{\sigma}^q(\mathbf{s}) = \xi^q(\mathbf{s}) + f_\epsilon^q\phi_\epsilon^q(\mathbf{s}) = \xi^q(\mathbf{s}) + \left(2f_\epsilon|\hat{\mathbf{h}}:\mathbf{s}|\right)^q = \sigma_r^q \tag{27}$$

where the function ξ is defined as follows:

$$\xi(\mathbf{s}) = \sqrt{\phi^2\left(\mathbf{s_c} + \frac{1}{g_L}\mathbf{s_o}\right) + \phi^2\left(\frac{k_P(1-g_S)}{g_L}\mathbf{s_o}\right)} \tag{28}$$

with a suggested value of 4 for the parameter k_P. Defining the following deviatoric components,

$$\mathbf{s}' = \mathbf{s_c} + \frac{1}{g_L}\mathbf{s_o} \tag{29}$$

$$\mathbf{s}'' = \frac{k_P[1-g_S]}{g_L}\mathbf{s_o} \tag{30}$$

and replacing into Eq. (28) an alternative expression for ξ is obtained:

$$\xi^2 = \phi^2(\mathbf{s}') + \phi^2(\mathbf{s}'') \tag{31}$$

In general $g_L \geqslant 1$ and $g_S \leqslant 1$ but when no latent effects exist ($g_L = g_S = 1$), the function $\xi(\mathbf{s})$ reduces to $\phi(\mathbf{s})$ and the original model in (6) is recovered. Furthermore, since ξ is also positively homogeneous to first degree, Eq. (14) can be re-written for the extended function:

$$f_\omega = \frac{H\xi(\omega\hat{\mathbf{h}})}{2}\left[\left(\frac{s_{\epsilon i}}{s_{\omega d}}\frac{\xi(\epsilon\hat{\mathbf{h}})}{\xi(\omega\hat{\mathbf{h}})}\right)^q - 1\right]^{\frac{1}{q}} \tag{32}$$

As a consequence, all cases investigated in Section 2.4 are equally valid for the extended yield function.

3.3. Coaxial stress states

If the stress state is coaxial with the microstructure deviator, i.e. $\mathbf{s_o} = 0$ and $\mathbf{s} = \mathbf{s_c}$, substituting into Eq. (28) prove that the extension reduces to the original yield locus

$$\xi(\mathbf{s_c}) = \xi(\mathbf{s}) = \phi(\mathbf{s}) \tag{33}$$

As mentioned in Sections 2.3 and 2.4, if the stress state is proportional, the products $\phi_+ f_+$ and $\phi_- f_-$ will be both null. Hence using Eqs. (27) and (33) it is seen that, for proportional loading, the equality $\bar{\sigma} = \phi$ is also valid for the extended yield condition.

3.4. Orthogonal stress states

For a stress state orthogonal to the microstructure deviator, i.e. $\hat{\mathbf{h}}:\mathbf{s} = 0$ or $\mathbf{s} = \mathbf{s_o}$, the application of Eqs. (27) and (28) demonstrates that, the yield condition does not depend on the state variables f_-, f_+, that is:

$$\bar{\sigma}(\mathbf{s}) = \xi(\mathbf{s}) = \frac{\sqrt{1 + k_P^2(1-g_S)^2}}{g_L}\phi(\mathbf{s_o}) = \sigma_r \tag{34}$$

There are many possible states orthogonal to $\hat{\mathbf{h}}$. For instance those indicated in Fig. (1), which intersect the stable and distorted yield surfaces respectively at $\mathbf{s_{oi}} = s_{oi}\sqrt{H}\hat{\mathbf{s}}$ and $\mathbf{s_{od}} = s_{od}\sqrt{H}\hat{\mathbf{s}}$. As both states refer to the same reference stress σ_r, the equality $\xi(\mathbf{s_{od}}) = \phi(\mathbf{s_{oi}})$ must hold. Thus replacing into (34) the following is obtained:

$$\frac{\sqrt{1 + k_P^2(1-g_S)^2}}{g_L}s_{od}\sqrt{H}\phi(\hat{\mathbf{s}}) = s_{oi}\sqrt{H}\phi(\hat{\mathbf{s}}) \tag{35}$$

Simplifying and rearranging:

$$\frac{s_{od}}{s_{oi}} = \frac{g_L}{\sqrt{1 + k_P^2(1-g_S)^2}} \tag{36}$$

If a single load change is considered and no cross-loading contraction is present ($g_S = 1$) the variable g_L is equal to the stress ratio.

In the absence of latent hardening though, the relationship between g_S and the stress ratio is nonlinear. The reason is that g_L is only active when load change has occurred, as latent hardening results in an overshoot of the monotonous flow curve. Whereas, in case of latent contraction the yield stress needs to be already reduced at the time of load path change and thus g_S needs to be active during the first deformation as well.

4. Interpretation of yield locus normal

If associative flow is assumed, the yield locus normal is known to be proportional to the incremental strain tensor. This means, in turn, that the strain distribution in any plastically deformed area will directly depend on the yield locus normal. In the presence of microstructure driven effects, particularly for non proportional loading, the evolution of the normal is unclear. For distortional hardening, e.g. with the HAH model, the yield locus shape changes, leading to variations in its normal. The minimal condition which needs to be satisfied here, is that distortion does not cause a change in the normal direction in case of proportional loading. The latter condition will be demonstrated in the following to hold for the HAH model and different cases will be discussed.

The expression for the yield surface normal can be obtained by deriving Eq. (27) with respect to the stress deviator:

$$\frac{\partial\bar{\sigma}}{\partial\mathbf{s}}=\left(\frac{\xi}{\bar{\sigma}}\right)^{q-1}\frac{\partial\xi}{\partial\mathbf{s}}+f_{\epsilon}^{q}\left(\frac{\phi_{\epsilon}}{\bar{\sigma}}\right)^{q-1}\frac{\partial\phi_{\epsilon}}{\partial\mathbf{s}} \tag{37}$$

Considering the expressions (29)–(31) the partial derivative of ξ with respect to the stress deviator takes the form

$$\frac{\partial\xi}{\partial\mathbf{s}}=\frac{\phi(\mathbf{s}')}{\xi(\mathbf{s})}\frac{\partial\phi(\mathbf{s}')}{\partial\mathbf{s}'}:\frac{\partial\mathbf{s}'}{\partial\mathbf{s}}+\frac{\phi(\mathbf{s}'')}{\xi(\mathbf{s})}\frac{\partial\phi(\mathbf{s}'')}{\partial\mathbf{s}''}:\frac{\partial\mathbf{s}''}{\partial\mathbf{s}} \tag{38}$$

with

$$\frac{\partial\mathbf{s}'}{\partial\mathbf{s}}=H\hat{\mathbf{h}}\otimes\hat{\mathbf{h}}+\frac{1}{g_L}[\mathbf{I_4}-H\hat{\mathbf{h}}\otimes\hat{\mathbf{h}}] \tag{39}$$

$$\frac{\partial\mathbf{s}''}{\partial\mathbf{s}}=\frac{k_P[1-g_S]}{g_L}[\mathbf{I_4}-H\hat{\mathbf{h}}\otimes\hat{\mathbf{h}}] \tag{40}$$

Finally, a simple derivation of the function ϕ_{ϵ}

$$\frac{\partial\phi_{\epsilon}}{\partial\mathbf{s}}=2\,\mathrm{sgn}(\hat{\mathbf{h}}:\mathbf{s})\hat{\mathbf{h}}=2\epsilon\hat{\mathbf{h}} \tag{41}$$

concludes the list of the different terms needed. The appearance of H in the Eqs. (40) shall not suggest that the normal depends on its value. This is easily verified by considering the following facts:

- $\bar{\sigma}$ is independent of H as demonstrated in Eq. (22).
- since $\mathbf{s}'$ and $\mathbf{s}''$ are independent of H thus ξ and $\frac{\partial\xi}{\partial\mathbf{s}}$ do not depend on this coefficient either.
- The second term on the right hand side of Eq. (37), features the quantities f_{ϵ} (contains $\sqrt{H}$), ϕ_{ϵ} (contains $1/\sqrt{H}$) and the tensor $\frac{\partial\phi_{\epsilon}}{\partial\mathbf{s}}$ (of size $1/\sqrt{H}$). Multiplying this quantities clearly eliminate the effect of H.

4.1. Proportional loading

As hinted at in Section 2.3, for proportional loading $\phi_{\epsilon}=f_{-\epsilon}=0$. Since $\bar{\sigma}=\xi$ Eq. (37) becomes:

$$\frac{\partial\bar{\sigma}}{\partial\mathbf{s}}=\frac{\partial\xi}{\partial\mathbf{s}} \tag{42}$$

Furthermore, because $g_L=1$ during proportional loading and the stress deviator is coaxial to $\hat{\mathbf{h}}$, then $\mathbf{s}'=\mathbf{s_c}=\mathbf{s}$ and $\mathbf{s_o}=\mathbf{0}$. This, in turn, results in $\frac{\partial\mathbf{s}'}{\partial\mathbf{s}}=\mathbf{I_4}$ and $\mathbf{s}''=\phi(\mathbf{s}'')=0$, which simplify the equation for the normal to:

$$\frac{\partial\bar{\sigma}}{\partial\mathbf{s}}=\frac{\phi(\mathbf{s})}{\xi(\mathbf{s})}\frac{\partial\phi}{\partial\mathbf{s}} \tag{43}$$

Since $\xi(\mathbf{s})=\phi(\mathbf{s})$ for proportional loading, the final result $\frac{\partial\bar{\sigma}}{\partial\mathbf{s}}=\frac{\partial\phi}{\partial\mathbf{s}}$ is obtained, which proves that the yield surface normal remains equal to that of isotropic hardening, in case of proportional loading.

4.2. Load reversal

Again, using the coaxiality of $\mathbf{s}$ and $\hat{\mathbf{h}}$ and recognizing that for load reversal $\epsilon\equiv-$, the expression for the yield locus normal can be written as follows:

$$\frac{\partial\bar{\sigma}(\mathbf{s})}{\partial\mathbf{s}}=\left(\frac{\phi(\mathbf{s})}{\bar{\sigma}(\mathbf{s})}\right)^{q-1}\frac{\partial\phi(\mathbf{s})}{\partial\mathbf{s}}\left[H\hat{\mathbf{h}}\otimes\hat{\mathbf{h}}+\frac{1}{g_L}(\mathbf{I_4}-H\hat{\mathbf{h}}\otimes\hat{\mathbf{h}})\right]-2f_{-}^{q}\left(\frac{\phi_{-}(\mathbf{s})}{\bar{\sigma}(\mathbf{s})}\right)^{q-1}\hat{\mathbf{h}} \tag{44}$$

Defining an auxiliary function $\kappa(\mathbf{s})$ as,

$$\kappa(\mathbf{s})=\frac{\phi(\mathbf{s})}{\bar{\sigma}(\mathbf{s})} \tag{45}$$

and remembering that by definition $\bar{\sigma}^q=\phi^q+\phi_{\epsilon}^q$, furthermore assuming $g_L=1$ (this would mean that the stress state stayed coaxial long enough) Eq. (44) can be written as:

$$\frac{\partial\bar{\sigma}(\mathbf{s})}{\partial\mathbf{s}}=(\kappa)^{q-1}\frac{\partial\phi(\mathbf{s})}{\partial\mathbf{s}}-2f_{-}^{q}(1-\kappa^q)^{1-\frac{1}{q}}\hat{\mathbf{h}} \tag{46}$$

In case of load reversal ($\mathbf{s}=-\|\mathbf{s}\|\sqrt{H}\hat{\mathbf{h}}$), κ is a ratio independent of the stress deviator. In fact, by substitution into Eq. (45) leads to:

$$\kappa=\frac{\phi(-\|\mathbf{s}\|\sqrt{H}\hat{\mathbf{h}})}{\bar{\sigma}(-\|\mathbf{s}\|\sqrt{H}\hat{\mathbf{h}})}=\frac{\phi(-\hat{\mathbf{h}})}{\bar{\sigma}(-\hat{\mathbf{h}})} \tag{47}$$

This fact enables the interpretation of the normal under load reversal. It can be recognized from Eq. (46) that the normal of the distorted surface is a linear combination (w.r.t. $\mathbf{s}$) of the normal of its isotropic counterpart and the tensor $\hat{\mathbf{h}}$. This means that even if ϕ is centro-symmetric the normal during load reversal does not correspond to that predicted by isotropic hardening.

4.3. Cross-loading

Similarly, considering cross loading, $\mathbf{s_o}=\mathbf{s},\mathbf{s_c}=0$ and $\phi_{\epsilon}=0$, thus Eqs. (29) and (30) become:

$$\mathbf{s}'=\frac{1}{g_L}\mathbf{s} \tag{48}$$

$$\mathbf{s}''=\frac{k_P[1-g_S]}{g_L}\mathbf{s} \tag{49}$$

Substituting the derivatives of these expressions into Eq. (38) and using the homogeneity of the functions the expression for the yield locus normal is obtained:

$$\frac{\partial\bar{\sigma}(\mathbf{s_o})}{\partial\mathbf{s}}=\frac{\sqrt{1+k_P^2(1-g_S)^2}}{g_L}\frac{\partial\phi(\mathbf{s_o})}{\partial\mathbf{s}} \tag{50}$$

This means that, for cross loading the direction of the normal is preserved but its size is stretched depending on the actual values of g_L and g_S to ensure work equivalence.

5. State variable evolution equations

The derivation of the evolution equations can be found in previous publications (i.e. Barlat et al., 2011, 2013, 2014). These are only

be repeated here for sake of completeness and commented as necessary. As mentioned in the previous sections the state variables g_-, g_+, g_L and g_S are all related to the ratio between two coaxial stress points in the distorted and isotropic yield surfaces. Furthermore, the microstructure deviator is a function of its angle with the current stress deviator. All of these variables are assumed to evolve as functions of the specific plastic work:

$$dw = \bar{\sigma} d\bar{\varepsilon} = \sigma_r d\bar{\varepsilon} = \sigma_{ij} d\varepsilon_{ij} \tag{51}$$

5.1. Evolution of the microstructure deviator

The microstructure deviator $\hat{\mathbf{h}}$, is initialized as the normalized stress deviator $\hat{\mathbf{s}}$ corresponding to the first plastic deformation increment and stays as such, as long as the loading stays proportional. If loading is reversed, the microstructure deviator also remains unaffected, as it is still coaxial to the stress deviator. Therefore, $\hat{\mathbf{h}}$ only evolves if $|\cos\chi| \neq 1$. Furthermore, the evolution law must be devised in a manner that $\hat{\mathbf{h}}$ always tends towards the current normalized stress deviator $\hat{\mathbf{s}}$ or it opposite $-\hat{\mathbf{s}}$. This is dictated by the fact that latent and Bauschinger effects are only transient and the flow stress eventually returns to the monotonic hardening curve. An evolution equation satisfying these requirements can be written as follows:

$$\frac{d\hat{\mathbf{h}}}{d\bar{\varepsilon}} = k \operatorname{sgn}(\cos\chi)[|\cos\chi|^{1/R} + g_R](\hat{\mathbf{s}} - \cos\chi\hat{\mathbf{h}}) \tag{52}$$

where

$$\frac{dg_R}{d\bar{\varepsilon}} = k_R[k'_R(1-\cos^2\chi) - g_R] \tag{53}$$

Note that Eq. (52) corresponds to Eq. (23) in Barlat et al. (2014), although this expression is not correct in that article. This can be easily inferred from g_R, which is, per definition, size independent and can be added only to size independent quantities. Thus, the parameter H appearing in the mentioned paper would violate this requirement.

Whether the proposed initialization for the tensor $\hat{\mathbf{h}}$ is optimal, is still an open question. The motivation for the choice made in this and the previous works is simplicity. On the other hand, how $\hat{\mathbf{h}}$ is initialized does not sensitively affect the response of the model. This is because the yield locus shape changes only gradually as a function of the state variables. Therefore even if $\hat{\mathbf{h}}$ were to be initialized arbitrarily (e.g. due to initial fluctuation in an FEM computation), as long as the initial path is not sustained over a considerable plastic strain range, the state variables will not be affected considerably. Additionally, once the deformation is stabilized to a particular path, $\hat{\mathbf{h}}$ will relatively quickly adjust itself to the new stress state, ensuring that only differences in sustained deformation paths are sensitively reflected to the result. Alternative initialization strategies, such as the relaxation of the constant size of $\hat{\mathbf{h}}$ or an increased rotation rate at small plastic strains might help minimize this effects. These are, however, out of the scope of the present contribution.

5.2. Evolution of the state variables related to Bauschinger effect and permanent softening

The Bauschinger effect and permanent softening evolutions (g_-, g_+, g^p_- and g^p_+)[2] depend on the sign of $\hat{\mathbf{h}} : \mathbf{s}$:

$$\begin{array}{ll} \text{If } \hat{\mathbf{h}}^s : \mathbf{s} \geqslant 0 & \text{If } \hat{\mathbf{h}}^s : \mathbf{s} < 0 \\ \frac{dg_-}{d\bar{\varepsilon}} = k_2\left(k_3\frac{\bar{\sigma}_0}{\bar{\sigma}} - g_-\right) & \frac{dg_-}{d\bar{\varepsilon}} = k_1\left(\frac{g^p_- - g_-}{g_-}\right) \\ \frac{dg_+}{d\bar{\varepsilon}} = k_1\left(\frac{g^p_+ - g_+}{g_+}\right) & \frac{dg_+}{d\bar{\varepsilon}} = k_2\left(k_3\frac{\bar{\sigma}_0}{\bar{\sigma}} - g_+\right) \\ \frac{dg^p_-}{d\bar{\varepsilon}} = k_5\left(k_4 - g^p_-\right) & \frac{dg^p_+}{d\bar{\varepsilon}} = k_5\left(k_4 - g^p_+\right) \end{array} \tag{54}$$

These evolution laws are designed in a manner to fulfill the following conditions:

- All state variables are initialized to 1.0 ($g_- = g_+ = g^p_- = g^p_+ = 1.0$).
- In case of monotonic loading, the state variable representing the stress states on the same side of the yield locus g_ϵ (with $\epsilon = sgn(\hat{\mathbf{h}} : \mathbf{s})$) stays identically equal to 1.0. In contrast, the stress ratio for the opposite side of the yield locus ($g_{-\epsilon}$) starts decreasing asymptotically towards $k_3(\bar{\sigma}_0/\bar{\sigma})$ with a rate controlled by k_2. Similarly, for permanent softening, the stress ratio representing the softening of the opposite side ($g^p_{-\epsilon}$) starts decreasing towards the saturation value of k_4 with a rate prescribed by k_5.
- If load reversal occurs, ϵ changes sign and the effect described in the previous bullet item is now valid for the opposite side of the yield locus. Furthermore, the stress ratio on the same side of the yield locus (g_ϵ), now starts to increase back towards the asymptote value of 1.0 (full recovery) or g^p_ϵ (permanent softening) with a rate prescribed by the parameter k_1.

5.3. Evolution of the state variables for latent effects

The state variable g_L varies according to:

$$\frac{dg_L}{d\bar{\varepsilon}} = k_L\left[\frac{\bar{\sigma} - \bar{\sigma}_0}{\bar{\sigma}}\left(\sqrt{L(1-\cos^2\chi) + \cos^2\chi} - 1\right) + 1 - g_L\right] \tag{55}$$

In case of proportional loading or load reversal the variable g_L stays at its initial value of 1.0. In fact, substituting $\cos^2\chi = 1$ in Eq. (55) leads to $dg_L/d\bar{\epsilon} = 0$, whereas for cross loading ($cos\chi = 0$), g_L first increases up to a maximum value and then decreases asymptotically towards 1.0, with a rate depending on the parameter k_L.

The state variable g_S instead is given as follows:

$$\frac{dg_S}{d\bar{\varepsilon}} = k_S[1 + (S-1)\cos^2\chi - g_S] \tag{56}$$

It is worth noting that g_S is already active during proportional loading. In fact, substituting $\cos^2\chi = 1$ in Eq. (56) it is observed that g_S asymptotically decreases to the value S with a rate given by k_S. For cross-loading ($cos\chi = 0$), g_S asymptotes to 1.0, again with a rate prescribed by k_S.

Initial values for all the state variables are given in Table 1 and Table 2 summarizes suggested values for the model coefficients.

5.4. Limit cases

Irrespective of the material history, the HAH model converges to a steady state, if the last deformation path remains unchanged sufficiently long. This can be inferred by taking the limit of the evolution equations with $\bar{\varepsilon} \to \infty$. In fact, as previously mentioned, these laws represent a saturation by design, meaning that

$$\lim_{\bar{\varepsilon}\to\infty} \frac{\partial \Sigma}{\partial \bar{\varepsilon}} = 0 \tag{57}$$

for all state variables Σ. Furthermore if no permanent softening is present this state corresponds to the isotropic hardening response.

[2] Note that for ease of explanation the notation here is chosen to differ from the previous publications. The correspondence is such that $g^p_+ = g_3$ and $g^p_- = g_4$. The upper index p stands for "permanent softening".

Table 1
State variable initial values.

Variable	g_1	g_2	g_3	g_4	g_L	g_S	g_R	$\hat{\mathbf{h}}$
Initial value	1.0	1.0	1.0	1.0	1.0	1.0	0	$\hat{\mathbf{s}}$ at first plastic increment

Table 2
Suggested and typical values for HAH model parameters.

Coefficients	Suggested	Typical[a]	Remark
H[b]			Controls the size of $\hat{\mathbf{h}}$
q	2		Yield surface curvature
k_1		20.–200.	Bauschinger effect
k_2		10.–100.	
k_3		0.1–1.	
k_4		0.8–1.	Permanent softening
k_5		1.–10.	
L		1.–2.	Latent hardening
k_L		100.–500.	
S		0.4–1.	Cross-loading contraction
k_S		5.–50.	
k_P	4		
k		15.–150.	Evolution of $\hat{\mathbf{h}}$
R	5		
k_R	15		
k'_R	0.2		

[a] Only meant as a suggestion. The actual value may lie outside this range.
[b] The value of H does not influence the model.

Table 3
Isotropic hardening parameters according to Hockett–Sherby model.

A	B	M	n
346.0	920.0	3.15	0.55

6. Examples

The theoretical results demonstrated in the previous sections are exemplified in this section.

6.1. Material properties

The deformation of a hypothetical material, with constitutive coefficients depicted in this section is considered for this purpose, in order to accentuate the different effects such as anisotropy and distortional hardening.

6.1.1. Isotropic hardening

The material is assumed to harden according to the Hockett–Sherby law which reads:

$$\sigma_r = B - (B - A)\exp(-M\bar{\varepsilon}^n) \tag{58}$$

The corresponding parameters are given in Table 3.

6.1.2. Yield locus

A Yld2000-2d model (see Barlat et al., 2003 for the model details) has been used as the stable yield function (ϕ) using a yield locus exponent $a = 8$ and the anisotropy parameters (α_{1-8}) listed in Table 4. The HAH model parameters are summarized in Table 5.

Table 4
Parameters for Yld2000-2d model used as stable yield function in HAH model.

α_1	α_2	α_3	α_4
0.486516	1.378348	0.753647	1.024595
α_5	α_6	α_7	α_8
1.036274	0.903645	1.232146	1.485802

6.2. Results

Two load cases are considered in order to analyze the states discussed in this article. The first case consists of 10% prestrain in uniaxial tension followed by uniaxial compression, both in rolling direction (RD). In the second case, plane strain tension in the RD is followed the uniaxial tension in transverse direction (TD).

6.2.1. Hardening behavior

Fig. 2 depicts the hardening behavior predicted by the mentioned HAH model for load reversal. It can be recognized in Fig. 2(a) that, after reversal the yield stress is considerably lower than the unloading flow stress. However, it recovers the monotonic curve with continued straining. For cross loading, the load change results in a stress overshoot due to latent hardening, which however vanishes with increasing strain (see Fig. 2(b)).

6.2.2. Yield locus shape

The evolution of the yield loci, represented in the π-plane, can be seen in Fig. 3. For load reversal, the region opposite to the direction of the stress tensor is distorted, whereas the region around the active stress state remains intact. The whole yield locus is, furthermore, enlarged due to isotropic hardening. In Fig. 3(b) the combined effect of latent hardening and cross loading contraction can be observed. In fact, right after plane strain loading, the yield locus is contracted in the direction orthogonal to this loading. Right at load reversal, however, latent hardening gets activated, which quickly compensates for the contraction and even generates an overshoot with respect to proportional loading (see 12.5% curve in Fig. 2(b)). After continued straining, the microstructure deviator tends to realign itself with the stress deviator corresponding to uniaxial tension in the TD, leading the yield locus to return on the isotropic hardening response near this stress state.

6.2.3. Evolution of R-values

The Lankford coefficient or R-value, the width-to-thickness strain ratio in uniaxial tension, is an indicator of the evolution of the yield locus normal. Inspecting Fig. 4 immediately indicates that the HAH model causes abrupt changes in the R-value after a load change. This consequently demonstrates that, substantial changes in the strain distribution should be expected in case of non-proportional loading. Although it is known that the R-value does not stay constant after a load change, it is still necessary to verify whether

Table 5
HAH model parameters.

Exp.	Evolution of $\hat{\mathbf{h}}$				Bauschinger effect					Latent effects				
q	k	R	k_R	k'_R	k_1	k_2	k_3	k_4	k_5	L	k_L	S	k_S	k_P
2	20	5	15	0.2	150	75	0.9	1	1	1.6	350	0.8	60	4

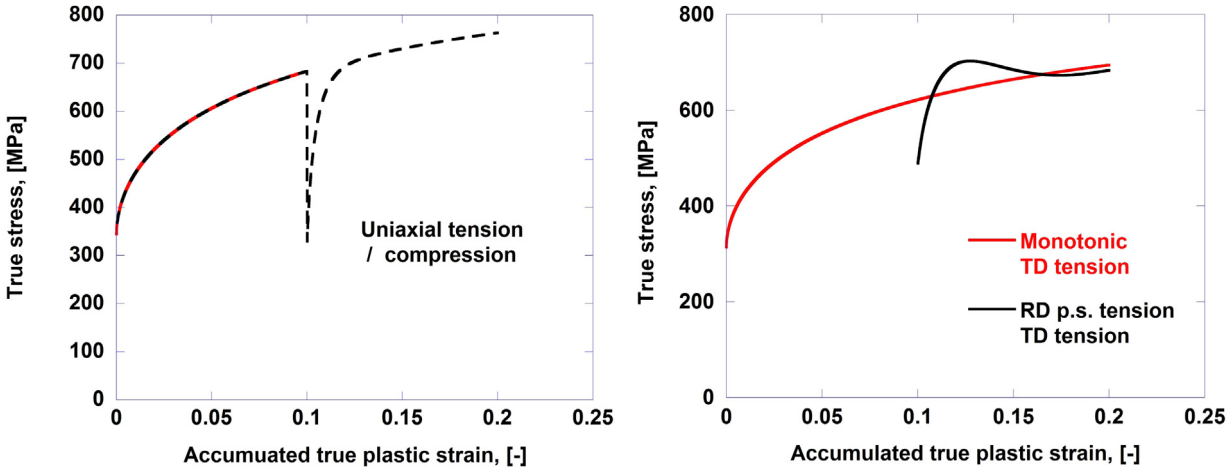

(a) Uniaxial tension-compression (b) Plane strain + uniaxial tension

Fig. 2. Hardening behavior.

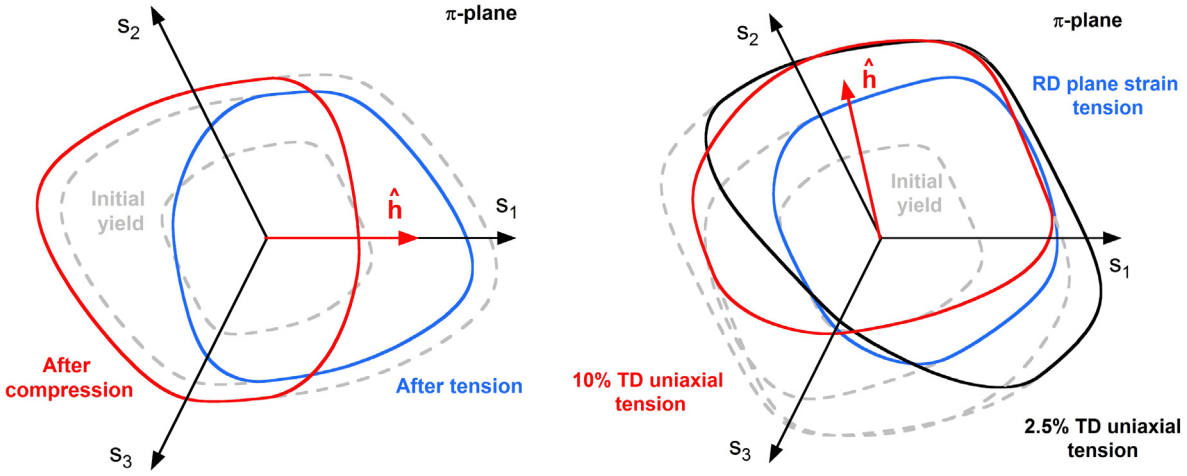

(a) Uniaxial tension-compression (b) Plane strain + uniaxial tension

Fig. 3. Yield locus shape.

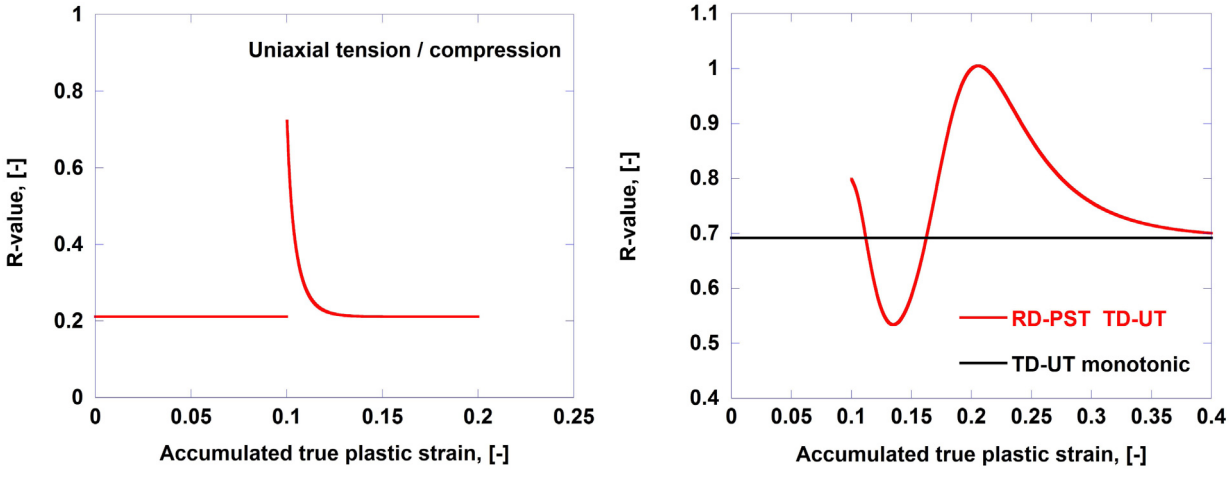

(a) Uniaxial tension-compression (b) Plane strain + uniaxial tension

Fig. 4. R-Value evolution.

this change is abrupt or gradual. In both loading cases investigated, it can be observed that the R-value eventually returns to the monotonic values. This demonstrates that the model is conservative in the sense that if the stress state remains proportional for a sufficiently large strain, it will behave like monotonic loading, irrespective of the previous loading history.

7. Conclusions

The present article provides a thorough discussion of the HAH model proposed and extended in Barlat et al. (2011), Barlat et al. (2013) and Barlat et al. (2014). The different aspects of the model are analytically discussed in order to improve the understanding of the model and facilitate its use. In particular the following conclusions can be drawn:

- The HAH approach is a modular framework, which allows the modeling of anisotropy, Bauschinger effect, latent hardening and cross-loading contraction. These effects are completely uncoupled from each other and can be modeled separately or combined arbitrarily with the corresponding variables.
- It is demonstrated that the model preserves the same flow stress and yield surface normal as that predicted with isotropic hardening, in the case of proportional loading. This is, however, not the case for load reversal or cross-loading. In fact, it can be seen from the development of the R-value, that during transient Bauschinger effect or latent hardening/softening, this value fluctuates quite strongly. This, in turn, implies that the strain distribution must differ substantially depending on the hardening assumption (HAH or isotropic) after load change.
- It is proven that the HAH response always tends towards that of isotropic hardening, no matter how complex the previous deformation history is, if the final loading is sustained sufficiently long, except in the case of permanent softening.

References

Aretz, H., 2008. A simple isotropic-distortional hardening model and its application in elastic-plastic analysis of localized necking in orthotropic sheet metals. Int. J. Plast 24 (9), 1457–1480, cited By (since 1996)35.

Barlat, F., Brem, J., Yoon, J., Chung, K., Dick, R., Lege, D., Pourboghrat, F., Choi, S.-H., Chu, E., 2003. Plane stress yield function for aluminum alloy sheets part 1: theory. Int. J. Plast 19 (9), 1297–1319, doi:<http://dx.doi.org/10.1016/S0749-6419(02)00019-0>.

Barlat, F., Gracio, J.J., Lee, M.-G., Rauch, E.F., Vincze, G., 2011. An alternative to kinematic hardening in classical plasticity. Int. J. Plast 27 (9), 1309–1327.

Barlat, F., Ha, J., Grácio, J.J., Lee, M.-G., Rauch, E.F., Vincze, G., 2013. Extension of homogeneous anisotropic hardening model to cross-loading with latent effects. Int. J. Plast 46, 130–142.

Barlat, F., Vincze, G., Grácio, J., Lee, M.-G., Rauch, E., Tomé, C., 2014. Enhancements of homogenous anisotropic hardening model and application to mild and dual-phase steels. Int. J. Plast 58, 201–218.

Chaboche, J., 2008. A review of some plasticity and viscoplasticity constitutive theories. Int. J. Plast. 24 (10), 1642–1693, special Issue in Honor of Jean-Louis Chaboche. doi:<http://dx.doi.org/10.1016/j.ijplas.2008.03.009>.

Dafalias, Y., Feigenbaum, H., 2011. Biaxial ratchetting with novel variations of kinematic hardening. Int. J. Plast 27 (4), 479–491, cited By (since 1996)11.

Feigenbaum, H., Dafalias, Y., 2007. Directional distortional hardening in metal plasticity within thermodynamics. Int. J. Solids Struct. 44 (22–23), 7526–7542, cited By (since 1996)30.

Feigenbaum, H., Dafalias, Y., 2008. Simple model for directional distortional hardening in metal plasticity within thermodynamics. J. Eng. Mech. 134 (9), 730–738, cited By (since 1996)18.

Franz, G., Abed-Meraim, F., Ben Zineb, T., Lemoine, X., Berveiller, M., 2009. Role of intragranular microstructure development in the macroscopic behavior of multiphase steels in the context of changing strain paths. Mater. Sci. Eng., A 517 (1–2), 300–311, cited By (since 1996)9.

Ha, J., Lee, J., Kim, J.H., Barlat, F., Lee, M.-G., 2014. Mesoscopic analysis of strain path change effect on the hardening behavior of dual-phase steel. Steel Res. Int. 85 (6), 1047–1057. http://dx.doi.org/10.1002/srin.201300186, URL <http://dx.doi.org/10.1002/srin.201300186>.

Ha, J., Kim, J.-H., Barlat, F., Lee, M.-G., 2014. Continuous strain path change simulations for sheet metal. Comput. Mater. Sci. 82, 286–292, doi:<http://dx.doi.org/10.1016/j.commatsci.2013.09.042>.

Hariharan, K., Barlat, F., Lee, M.G., Prakash, R.V., 2014. Extension of strainlife equation for low-cycle fatigue of sheet metals using anisotropic yield criteria and distortional hardening model. Fatigue Fract. Eng. Mater. Struct., n/a–n/a<http://dxdoi.org/10.1111/ffe.12162>. URL <http://dx.doi.org/10.1111/ffe.12162>.

He, W., Zhang, S., Song, H., 2013. An extended homogenous yield function based anisotropic hardening model for description of anisotropic hardening behavior of materials. Int. J. Mech. Sci. 77, 343–355, doi:<http://dx.doi.org/10.1016/j.ijmecsci.2013.05.018>.

Khan, A.S., Kazmi, R., Pandey, A., Stoughton, T., 2009. Evolution of subsequent yield surfaces and elastic constants with finite plastic deformation. Part-i: a very low work hardening aluminum alloy (al6061-t6511). Int. J. Plast 25 (9), 1611–1625, exploring New Horizons of Metal Forming Research. doi:<http://dx.doi.org/10.1016/j.ijplas.2008.07.003>.

Khan, A.S., Pandey, A., Stoughton, T., 2010. Evolution of subsequent yield surfaces and elastic constants with finite plastic deformation. Part ii: a very high work hardening aluminum alloy (annealed 1100 al). Int. J. Plast. 26 (10), 1421–1431, doi:<http://dx.doi.org/10.1016/j.ijplas.2009.07.008>.

Kitayama, K., Tom, C., Rauch, E., Gracio, J., Barlat, F., 2013. A crystallographic dislocation model for describing hardening of polycrystals during strain path changes. application to low carbon steels. Int. J. Plast 46 (0), 54–69, microstructure-based Models of Plastic Deformation. doi:<http://dx.doi.org/10.1016/j.ijplas.2012.09.004>.

Kurtyka, T., Zyczkowski, M., 1996. Evolution equations for distortional plastic hardening. Int. J. Plast 12 (2), 191–213, cited By (since 1996)31. URL <http://www.scopus.com/inward/record.url?eid=2-s2.0-0029702508&partnerID=40&md5=2e838ef621629f7db30b65cdd272fd4f>.

Lee, J.-Y., Lee, J.-W., Lee, M.-G., Barlat, F., 2012. An application of homogeneous anisotropic hardening to springback prediction in pre-strained u-draw/bending. Int. J. Solids Struct. 49 (25), 3562–3572, new Challenges in Mechanics & Materials for Sheet Metal Forming. doi:<http://dx.doi.org/10.1016/j.ijsolstr.2012.03.042>.

Lee, J.-W., Lee, M.-G., Barlat, F., 2012. Finite element modeling using homogeneous anisotropic hardening and application to spring-back prediction. Int. J. Plast 29, 13–41, doi:<http://dx.doi.org/10.1016/j.ijplas.2011.07.007>.

Lee, J., Lee, J.-Y., Barlat, F., Wagoner, R., Chung, K., Lee, M.-G., 2013. Extension of quasi-plastic–elastic approach to incorporate complex plastic flow behavior application to springback of advanced high-strength steels. Int. J. Plast 45 (0), 140–159, in Honor of Rob Wagoner. doi:<http://dx.doi.org/10.1016/j.ijplas.2013.01.011>.

Ortiz, M., Popov, E.P., 1983. Distortional hardening rules for metal plasticity. J. Eng. Mech. 109 (4), 1042–1057, cited By (since 1996)23. URL <http://www.scopus.com/inward/record.url?eid=2-s2.0-0020799575&partnerID=40&md5=53b1f7b954d9d1f6ab2672c89075e112>.

Peeters, B., Kalidindi, S., Van Houtte, P., Aernoudt, E., 2000. A crystal plasticity based work-hardening/softening model for b.c.c. metals under changing strain paths. Acta Mater. 48 (9), 2123–2133, cited By (since 1996)77.

Peeters, B., Seefeldt, M., Teodosiu, C., Kalidindi, S., Van Houtte, P., Aernoudt, E., 2001. Work-hardening/softening behaviour of b.c.c. polycrystals during changing strain paths: I. An integrated model based on substructure and texture evolution, and its prediction of the stress-strain behaviour of an if steel during two-stage strain paths. Acta Mater. 49 (9), 1607–1619, cited By (since 1996)133.

Phillips, A., Liu, C., Justusson, J., 1972. An experimental investigation of yield surfaces at elevated temperatures. Acta Mech. 14 (2–3), 119–146, cited By (since 1996)36. URL <http://www.scopus.com/inward/record.url?eid=2-s2.0-0015481341&partnerID=40&md5=487c27e8b75a6721d4cbe88ffaee37e4>.

Pietryga, M.P., Vladimirov, I.N., Reese, S., 2012. A finite deformation model for evolving flow anisotropy with distortional hardening including experimental validation. Mech. Mater. 44 (0), 163–173, microstructures and Anisotropies. doi:<http://dx.doi.org/10.1016/j.mechmat.2011.07.014>.

Shutov, A., Ihlemann, J., 2012. A viscoplasticity model with an enhanced control of the yield surface distortion. Int. J. Plast 39, 152–167, cited By (since 1996)4. URL <http://www.scopus.com/inward/record.url?eid=2-s2.0-84869082079&partnerID=40&md5=3f159e21a06c16019848e90f27c4b15f>.

Teodosiu, C., Hu, Z., 1998. Microstructure in the continuum modelling of plastic anisotropy. In: Proceedings of the Ris International Symposium on Material Science: Modelling of Structure and Mechanics of Materials from Microscale to Products, pp. 149–168 (Cited By (since 1996)52).

Voyiadjis, G.Z., Foroozesh, M., 1990. Anisotropic distortional yield model. J. Appl. Mech., Trans. ASME 57 (3), 537–547, cited By (since 1996)25.

Yoshida, F., Uemori, T., 2002. A model of large-strain cyclic plasticity describing the bauschinger effect and workhardening stagnation. Int. J. Plast 18 (5–6), 661–686, cited By (since 1996)173.

Yoshida, F., Uemori, T., 2003. A model of large-strain cyclic plasticity and its application to springback simulation. Int. J. Mech. Sci. 45 (10), 1687–1702, cited By (since 1996)130.

Yoshida, F., Uemori, T., Fujiwara, K., 2002. Elastic–plastic behavior of steel sheets under in-plane cyclic tension–compression at large strain. Int. J. Plast 18 (56), 633–659, doi:<http://dx.doi.org/10.1016/S0749-6419(01)00049-3>.